Eur. Phys. J. C 1, 293–300 (1998)

THE EUROPEAN PHYSICAL JOURNAL C

Open charm production in diffractive ep collisions

M. Diehl

Centre de Physique Théorique[a], Ecole Polytechnique, F-91128 Palaiseau Cedex, France (e-mail: diehl@orphee.polytechnique.fr)

Received: 10 January 1997 / Revised version: 17 February 1997

Abstract. The cross section for the diffractive reaction $\gamma^* + p \to c\bar{c} + p$ with a real or virtual photon is calculated in the nonperturbative two-gluon exchange model of Landshoff and Nachtmann. Numerical predictions are given for cross sections and spectra at typical HERA values of c.m. energy and photon virtuality. The contribution of charm to the diffractive structure function is evaluated and found to be rather small in the model, and the ratio between the production rates for $b\bar{b}$ and $c\bar{c}$ is tiny.

1 Introduction

The discovery of diffractive events in ep collisions at HERA [1] has triggered a large amount of experimental and theoretical work and greatly increased our knowledge of the physics of diffraction, or of the pomeron. Several models give a reasonable description of the data at the time being, but we are far yet from a coherent picture of the mechanisms at work in terms of QCD. One can hope that the detailed study of the diffractive final state will lead to further progress in this direction. Charm production looks promising in this respect, as predictions for this process differ widely between various models [2–6].

In this paper we use the approach due to Landshoff and Nachtmann (LN) to model the soft pomeron by the exchange of two nonperturbative gluons. We present differential cross sections for the diffractive dissociation of a real or virtual photon into a $c\bar{c}$-pair. Provided that the invariant mass of the diffractive final state is not too large its $c\bar{c}$-component should give a fair approximation of inclusive diffractive charm production. In the following section we give some details of the model and of the calculation, in Sect. 3 we present our results, and in Sect. 4 we summarise our findings.

2 Diffractive $c\bar{c}$-production in the LN model

The Landshoff-Nachtmann model has been introduced and described in [7,8]. It approximates the soft pomeron by the exchange of two *nonperturbative* gluons, with a propagator $-g_{\mu\nu}D(l^2)$ instead of the perturbative $-g_{\mu\nu}/l^2$ in Feynman gauge. In several processes one can express the scattering amplitude in terms of a few moments of the function $D(l^2)$ and thus does not need to know its detailed form. Here we only need the integral

$$\int_0^\infty dl^2 [\alpha_s^{(0)} D(-l^2)]^2 \cdot l^2 = \frac{9\beta_0^2\mu_0^2}{8\pi}\,, \tag{1}$$

where $\beta_0 \approx 2.0\,\mathrm{GeV}^{-1}$ and $\mu_0 \approx 1.1\,\mathrm{GeV}$ have been extracted from experimental data [8,9]. The parameter μ_0^2 provides the characteristic scale for the dependence of $D(l^2)$ on the gluon virtuality l^2, and $\alpha_s^{(0)}$ stands for the strong coupling in the nonperturbative region which dominates the l^2-integration in (1). It will be taken as $\alpha_s^{(0)} \approx 1$ here [9].

We now apply this model to the reaction

$$\gamma^* + p \to c\bar{c} + p\,. \tag{2}$$

In the following we use the conventional variables x, y, s, t, Q^2, W^2 for deep inelastic scattering, M for the invariant mass of the $c\bar{c}$-pair, and

$$\beta = \frac{Q^2}{Q^2 + M^2 - t}\,, \qquad \xi = \frac{Q^2 + M^2 - t}{W^2 + Q^2}\,. \tag{3}$$

We denote with P_T the transverse momentum of the charm quark with respect to the photon momentum in the $\gamma^* p$ c.m.

In the high-energy limit the scattering amplitude for our process is dominated by its imaginary part and we can use the cutting rules to calculate it. Then the diagrams contributing to (2) are those in Fig. 1 and the ones obtained by reversing the charge flow of the upper quark line. In each diagram there is one off-shell quark, the characteristic scale for its virtuality being given by [4,10]

$$\lambda^2 = \frac{P_T^2 + m_c^2}{1 - \beta}\,. \tag{4}$$

For charm production the large quark mass m_c protects this quark from becoming infrared so that a perturbative treatment of the quark sector should be safe, even in the photoproduction limit.

The cross section for photons with transverse or longitudinal polarisation in the $\gamma^* p$ frame has been calculated in [11,12]. It reads

[a] Unité propre 14 du CNRS

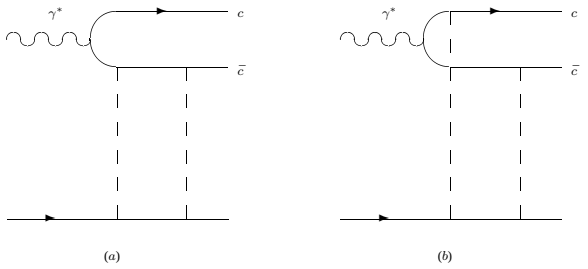

Fig. 1. Two of the four Feynman diagrams contributing to the imaginary part of the amplitude for $p+\gamma^* \to p+c\bar{c}$. The other two are obtained by reversing the charge flow of the upper quark line. The *lower line* stands for a constituent quark in the proton as explained in [11], and the *dashed lines* denote nonperturbative gluons

$$\frac{d\sigma_{T,L}}{dP_T^2\, dM^2\, dt} = \frac{16}{3}\,\alpha_{em} e_c^2\,\frac{\alpha_s(\lambda^2)}{\alpha_s^{(0)}}\,F_1^2(t)\,\xi^{2(1-\alpha_{I\!P}(t))} \times \frac{1}{(M^2+Q^2)^4}\,\frac{1}{\sqrt{1-4(P_T^2+m_c^2)/M^2}}\,\mathcal{S}_{T,L}\,, \qquad (5)$$

where $e_c = 2/3$ is the electric charge of the charm quark in units of the positron charge, and $F_1(t)$ the Dirac form factor of the proton. We have approximated $t = 0$ for the squared momentum transfer from the proton, except in $F_1(t)$ and $\alpha_{I\!P}(t)$, which accounts for most of the t-dependence in the cross section [12]. $\alpha_{I\!P}(t) \approx 1.085 + t/(2\ \mathrm{GeV})^2$ is the soft pomeron trajectory as observed in hadronic reactions [13]. It is introduced by hand in the LN model in order to make contact with experiment; the approximation of bare two-gluon exchange (Fig. 1) would give a factor ξ^0 instead of $\xi^{2(1-\alpha_{I\!P}(t))}$ in the cross section (5). We thus assume that the energy dependence of diffractive charm production is given by the soft pomeron, and furthermore that ξ is the correct dimensionless variable to be raised to the Regge power $(1/\xi)^{\alpha_{I\!P}(t)}$ in the amplitude. In our numerical applications we will impose an upper cut of $\xi \leq 0.05$ to remain in a region where the exchange of a pomeron dominates that of secondary trajectories.

The expressions

$$\mathcal{S}_T = \left(1 - 2\,\frac{P_T^2+m_c^2}{M^2}\right)\,\frac{P_T^2}{P_T^2+m_c^2}\,(M^2+Q^2)^2\,L_1(P_T^2,w)^2 + \frac{m_c^2}{P_T^2+m_c^2}\,(M^2+Q^2)^2\,L_2(P_T^2,w)^2$$
$$\mathcal{S}_L = 4\,\frac{Q^2}{M^2}\,\frac{P_T^2+m_c^2}{M^2}\,(M^2+Q^2)^2\,L_2(P_T^2,w)^2 \qquad (6)$$

in (5) contain integrals $L_1(P_T^2,w)$ and $L_2(P_T^2,w)$ over the virtuality of the exchanged gluons,

$$L_i(P_T^2,w) = \int_0^\infty dl^2\,[\alpha_s^{(0)} D(-l^2)]^2\,f_i(v,w)\,, \quad i=1,2 \qquad (7)$$

with

$$f_1(v,w) = 1 - \frac{1}{2w}\left[1 - \frac{v+1-2w}{\sqrt{(v+1-2w)^2+4w(1-w)}}\right]$$
$$f_2(v,w) = 1 - \frac{1}{\sqrt{(v+1-2w)^2+4w(1-w)}} \qquad (8)$$

and[1]

$$v = \frac{l^2}{\lambda^2}\,, \qquad w = \frac{P_T^2}{\lambda^2}\,. \qquad (9)$$

A simple way to approximate L_i is to Taylor expand the function $f_i(v,w)$ about $v = 0$ and to keep only the leading term

$$f_i(v,w) \approx v \cdot \left.\frac{\partial f_i(v,w)}{\partial v}\right|_{v=0}\,, \qquad (10)$$

after which the integrals reduce to the moment (1) of the gluon propagator. This is however not very good for small P_T^2, where the variable v becomes $v = (1-\beta)\cdot l^2/m_c^2$ so that one needs a good approximation of the functions $f_1(v)$, $f_2(v)$ for v from zero to order one. A better approximation which also leads to the moment (1) is

$$f_i(v,w) \approx \frac{v}{v_0}\cdot f_i(v_0,w)\,, \qquad v_0 = \frac{l_0^2}{\lambda^2} \qquad (11)$$

with $l_0^2 \sim \mu_0^2$. Whereas in (10) one approximates the curve $f_i(v)$ by its tangent at $v = 0$ the approximation (11) uses instead the line that intersects the curve at $v = 0$ and $v = v_0$, the corresponding range in l^2 from 0 to l_0^2 being the dominant region of integration in L_i. We have varied the parameter l_0^2 between $\mu_0^2/2$ and $2\mu_0^2$ and found variations of up to a factor 1.6 in the integrated $\gamma^* p$ cross sections σ_T and σ_L and variations of less than a factor 2.1 for cross sections differential in M^2 or in P_T^2, together with some change in the shape of the spectra. The effects are stronger at small or zero Q^2 and more pronounced in the P_T^2 - than in the M^2-spectra. These variations may be seen as reflecting our uncertainty about the exact shape of the nonperturbative gluon propagator, which determines the value of l_0^2 for which the approximation (11) is best. As a benchmark we have compared the approximated integrals with the exact ones for the model gluon propagator used in [8],

$$D(-l^2) \propto \left[1 + \frac{l^2}{(n-1)\mu_0^2}\right]^{-n}\,, \qquad n \geq 4\,, \qquad (12)$$

where the proportionality constant can easily be obtained from (1). With (11) the errors of the approximation stay below 10% for all P_T^2 and w we need, whereas the tangent approximation (10) has errors of 50% and more when one goes to $P_T^2 = 0$.

Finally a comment is in order about the value of the strong coupling in our calculation. In the integral (1) it is taken at a nonperturbative scale given by the dominant virtuality of the exchanged gluons. However, the first

[1] The definitions of v and w here differ from those in [11]

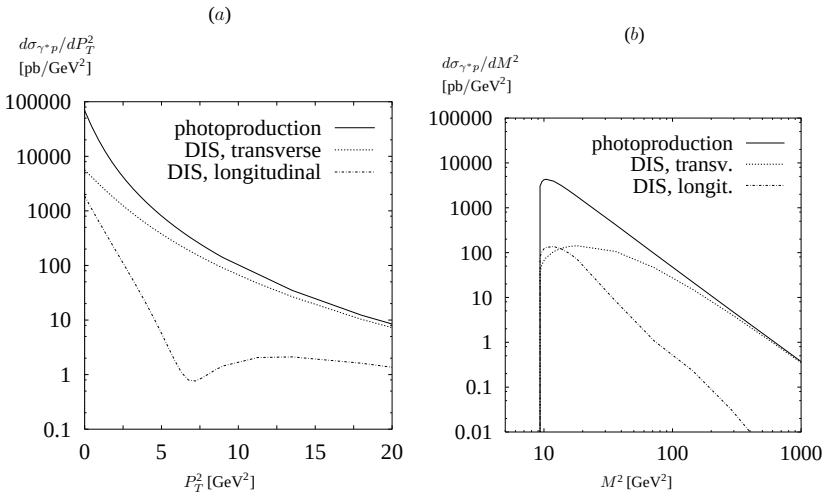

Fig. 2. Spectra in P_T^2 and in M^2 for $\gamma^* p \to c\bar{c}\,p$ at $W = 220$ GeV with a cut $\xi \leq 0.05$. The curves are for photoproduction and for electroproduction at $Q^2 = 20$ GeV^2 with transverse or longitudinal photons

gluon in all diagrams couples at its upper end to an off-shell quark whose virtuality is in the perturbative region. We choose to take the coupling for *this* vertex at the scale λ^2 in all four diagrams, and at the small gluonic scale for the other three vertices. One might argue that λ^2 is the typical scale for the entire upper parts of the diagrams, and that one should also take the coupling of the second gluon to the upper quark line at this scale. Note however that, since we use the cutting rules, the parts of the diagrams to the left and the right of the cut lines can be considered independently, and that the part to the right of the cut is just on-shell quark-quark or quark-antiquark scattering with no large virtuality involved. We are aware though that our choice is only a guess.

It is clear that this question of scales leads to an uncertainty in the normalisation of our predictions. The main problem is not so much whether λ^2 is the best choice of a hard scale, which is a common problem of all leading order calculations. Since the moment (1) includes the nonperturbative coupling $\alpha_s^{(0)}$ we have to multiply the cross section with $\alpha_s(\lambda^2)/\alpha_s^{(0)}$ if at one of the four quark-gluon vertices we take the perturbative coupling. $\alpha_s^{(0)}$ is not well constrained by phenomenology [9] or theory and other choices than $\alpha_s^{(0)} = 1$ which we adopt here have indeed been made [14].

3 Results

We will now give some numerical predictions for the diffractive production of charm. We stress once again that we calculate the cross section for the diffractive final state being a quark-antiquark pair, which does not include events with $c\bar{c}$ and additional gluons at parton level. It is also different from $c\bar{c}$-production through photon-gluon fusion where the gluon is a parton emitted by the pomeron in the description of Ingelman and Schlein [15] and where the final state contains a pomeron remnant. Finally it excludes events in photoproduction where the photon is resolved.

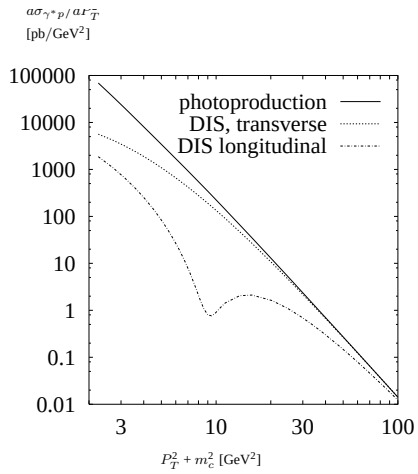

Fig. 3. The spectra of Fig. 2 **a** for a wider range in P_T^2, as a function of $P_T^2 + m_c^2$ in a double logarithmic plot. For photoproduction one recognises the power behaviour (13)

Let us start with photoproduction. For $W = 220$ GeV and $\xi \leq 0.05$ we obtain a total rate $\sigma(\gamma p \to c\bar{c}\,p) = 57$ nb. Spectra in P_T^2 and M^2 are shown in Fig. 2 and 3. The P_T^2-spectrum is well described by a power behaviour

$$\frac{d\sigma_{\gamma p}}{dP_T^2} \propto (P_T^2 + m_c^2)^{-\delta} \tag{13}$$

with an exponent δ between 3.7 and 4.3 in the P_T^2-range of Fig. 3. The spectrum of diffractive mass behaves approximately like $d\sigma_{\gamma p}/dM^2 \propto M^{-4.2}$ to the right of its peak.

Let us move on to electroproduction and first focus on the dependence on the $\gamma^* p$ c.m. energy W of the *ep* cross section, obtained from the usual relation

$$d\sigma_{ep} = \frac{\alpha_{em}}{\pi}\,\frac{dW^2}{W^2}\,\frac{dQ^2}{Q^2} \Big\{(1 - y + y^2/2)\,d\sigma_T + (1-y)\,d\sigma_L\Big\} \tag{14}$$

where we have used the approximation $x \ll 1$. It is determined by different effects:

1. the integration element dW^2/W^2 in (14)
2. the y-dependent factors multiplying $d\sigma_T$ and $d\sigma_L$, note that at $x \ll 1$ one has $y \approx W^2/s$. They decrease with W. As they are different for transverse and longitudinal photons one cannot calculate their effect without knowing the relative contribution of σ_T and σ_L. This problem is of course absent in the photoproduction limit.
3. the cut in ξ which ensures that the selected events are dominated by pomeron exchange. It leads to an upper limit on the diffractive mass M that depends on W and Q^2 and whose importance is strongest for small W and large Q^2. This effect can be circumvented by using a fixed cut on M chosen such that ξ is always small enough, but at the expense of the total rate used in the analysis.
4. the dependence on W of $d\sigma_{T,L}/(dP_T^2\, dM^2\, dt)$. This gives direct information about whether or not this process is dominated by the soft pomeron. In our model it comes from the factor $\xi^{2(1-\alpha_{I\!P}(t))}$ in (5), i.e. with $W^2 \gg Q^2$ it is $W^{4(\alpha_{I\!P}(t)-1)}$ which is quite flat given that the soft pomeron intercept is close to 1.

We find an ep cross section of 120 pb for $\sqrt{s} = 296$ GeV, $\xi \leq 0.05$, integrated over Q^2 from 7.5 GeV^2 to 80 GeV^2 and W from 50 GeV to 220 GeV. Table 1**a** gives the ep cross section in three different bins of W. They are spaced logarithmically to take out the trivial effect of point 1, above. One might also choose the binning to include the factor $1 - y + y^2/2$ if one assumes the longitudinal contribution to the cross section to be small; one then directly extracts the W-dependence of the integrated $\gamma^* p$ cross section σ_T. The effects of points 2 and 3 are responsible for the decrease of the cross section from the second to the third W-bin in our numerical example. Apart from this one sees however clearly the flat behaviour in W characteristic of soft pomeron exchange. It might be useful to analyse experimental data in this way: it focuses on the W-dependence of the $\gamma^* p$ cross section and apart from points 2 and 3 does not involve the details of its dependence on M^2 or Q^2, so it is relatively model independent. Also it requires only binning in one variable and thus makes best use of the available statistics which is likely not to be abundant at HERA. If there were a strong departure from the soft pomeron energy dependence for these events it should be seen in such an analysis.

In Table 1**b** we give the ep cross section in logarithmically spaced Q^2-bins. Since y is nearly independent of Q^2 at small x this directly shows the Q^2-dependence of the weighted sum of the integrated transverse and longitudinal $\gamma^* p$ cross sections.

Examples of ep spectra are shown in Fig. 4 and $\gamma^* p$ spectra for transverse and longitudinal photons in Fig. 2. In the M^2-spectrum of Fig. 2 **b** we can see that the contribution from longitudinal photons is much smaller than from transverse ones except at very small M^2. This is explained by the factor $(P_T^2 + m_c^2)/M^2$ in the differential cross section for longitudinal polarisation, cf. (6). The

Table 1. σ_{ep} for $ep \to ep\, c\bar{c}$ with $\sqrt{s} = 296$ GeV and $\xi \leq 0.05$. **a** For Q^2 from 7.5 GeV^2 to 80 GeV^2 and three logarithmically spaced bins in W. **b** For W from 50 GeV to 220 GeV and three logarithmic bins in Q^2

(*a*)

W[GeV]		
50 ... 82	82 ... 134	134 ... 220
39 pb	44 pb	40 pb

(*b*)

Q^2[GeV^2]		
7.5 ... 16.5	16.5 ... 36.3	36.3 ... 80
73 pb	36 pb	14 pb

P_T^2-spectrum for transverse photons is less steep than in photoproduction at its lower end, but at large P_T^2 it becomes similar in slope and normalisation.

The dip in the P_T^2-spectrum for longitudinal polarisation is a consequence of the zero in the longitudinal cross section at certain values of P_T^2 and M^2, a characteristic feature of the two-gluon exchange mechanism in this reaction [4,10,11]. This zero can occur for $w > 1/2$ because then the function $f_2(v)$ and thus the integrand of $L_2(P_T^2, w)$ change sign at $v = 2(2w-1)$, cf. (7) to (9). Using the approximation (10) we find $d\sigma_L/(dP_T^2\, dM^2) = 0$ at $w = 1/2$, which is underestimated but good enough for the purpose of our discussion. The corresponding value of M^2 decreases with P_T^2 and reaches its threshold $4(P_T^2 + m_c^2)$ at $P_T^2 = m_c^2 + Q^2/4$, i.e. at $P_T^2 = 7.25$ GeV^2 in Fig. 2 **a**. Then the effect of the zero on the M^2-integrated cross section is strongest, as we can see from the position of the dip. Unfortunately this dip becomes completely swamped in the ep spectrum by the transverse contribution, cf. Fig. 4 **a**, so that this effect is unlikely to be observed.

The M^2-spectra can be rewritten in terms of the charm contribution to the diffractive structure functions $F_2^{D(4)}$, $F_T^{D(4)}$ and $F_L^{D(4)}$, defined by

$$\frac{d\sigma_{ep}}{dx\, dQ^2\, d\xi\, dt} = \frac{4\pi\alpha_{em}^2}{xQ^4} \left[\left(1 - y + y^2/2\right) F_T^{D(4)} + (1-y)\, F_L^{D(4)} \right]$$

$$F_2^{D(4)} = F_T^{D(4)} + F_L^{D(4)}\,, \tag{15}$$

where T and L stand for the contributions of transverse and longitudinal photon polarisation as usual. These functions depend on the kinematic variables x, Q^2, ξ, t or, equivalently, on ξ, β, Q^2, t. In models with Regge factorisation this dependence factorises into

$$F_{T,L}^{D(4)}(\xi, \beta, Q^2, t) = f_{I\!P}(\xi, t) \cdot F_{T,L}^{I\!P}(\beta, Q^2, t)\,, \tag{16}$$

where in the partonic interpretation of Ingelman and Schlein [15] $f_{I\!P}(\xi, t)$ gives the pomeron flux from the proton and $F_{T,L}^{I\!P}(\beta, Q^2, t)$ are the structure functions of the pomeron.

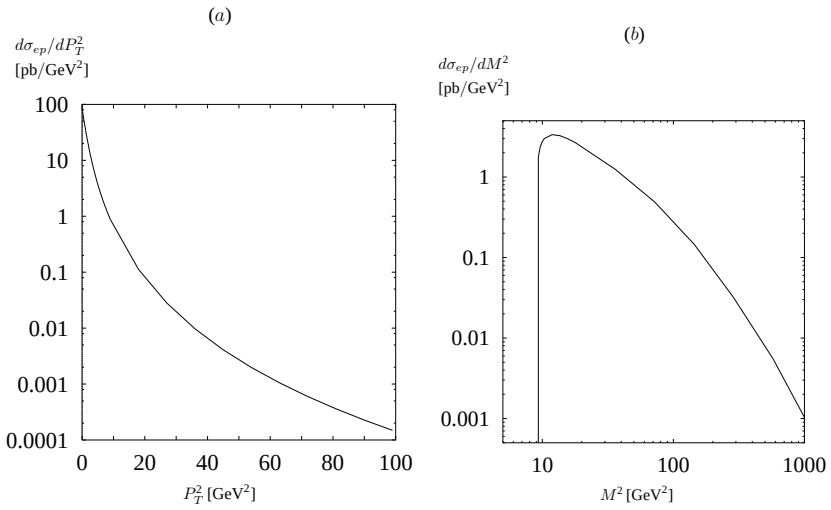

Fig. 4. Spectra in P_T^2 and in M^2 for $ep \to ep\,c\bar{c}$ at $\sqrt{s} = 296$ GeV, integrated over $\xi \leq 0.05$, $W = 50$ GeV to 220 GeV and $Q^2 = 7.5$ GeV^2 to 80 GeV^2

Our model has this factorisation property, but this is because it is put in rather than being one of its predictions: We calculate two-gluon exchange to leading order in ξ^{-1}, so that $F_{T,L}^{D(4)}(\xi, \beta, Q^2, t)$ depends on ξ via a global factor, and then we modify the exponent of ξ by hand introducing the soft pomeron trajectory, which preserves factorisation. Using the flux factor

$$f_{I\!P}(\xi, t) = \frac{9\beta_0^2}{4\pi^2} [F_1(t)]^2 \, \xi^{1-2\alpha_{I\!P}(t)} \tag{17}$$

we obtain the curves shown in Fig. 5 for the charm structure functions $F_T^{I\!P}(c\bar{c})$ and $F_L^{I\!P}(c\bar{c})$ of the pomeron. We observe that the transverse structure function shows Bjorken scaling for rather small β. It can be shown from the expressions (5) and (6) that $F_T^{I\!P}(c\bar{c})$ scales under the condition that the integrated cross section is dominated by values of P_T^2 that are small compared with the upper kinematical limit $M^2/4 - m_c^2$. Because with our values of Q^2 the diffractive mass M is not far from the production threshold $2m_c$ for moderate and large β this condition cannot be satisfied in this region and there is no scaling. Note also that at the value of β corresponding to $M = 2m_c$ both $F_T^{I\!P}(c\bar{c})$ and $F_L^{I\!P}(c\bar{c})$ vanish.

We wish to compare the rate of charm production with the inclusive diffractive cross section for light flavours u, d, s, which can also be calculated in our model [11,16]. Let us remark that for light flavours the quark virtuality λ^2 in (4) can become small so that one has to assume that a perturbative treatment of the quarks, possibly with an effective quark mass of some 100 MeV, is good enough for this process. We find that actually the best description of the HERA data with our model is obtained when just taking current masses for the u, d and s quarks [16], which we have done in the results to be shown. For light quarks the approximations (10) or (11) of the loop integrals L_1, L_2 can no longer be used unless P_T^2 is large so that one has to resort to a specific form of the gluon propagator $D(l^2)$. The results we show have been obtained using the model propagator (12) with $n = 4$ and freezing the running coupling $\alpha_s(\lambda^2)$ in (5) when it becomes equal to 1. $F_T^{I\!P}$ shows scaling over the entire β-range since there is no strong threshold effect as for charm at large β. The longitudinal structure function $F_L^{I\!P}$ is found to behave roughly like $1/Q^2$ at fixed β and only gives a significant contribution to $F_2^{I\!P}$ when β is large.

Figure 6 shows the result of our calculation of the ξ-integrated diffractive structure function $\tilde{F}_2^D(\beta, Q^2) = \int_{\xi_{min}}^{\xi_{max}} d\xi \int dt \, F_2^{D(4)}(\xi, \beta, Q^2, t)$ together with HERA data [17]. We only show one Q^2 per experiment as the dependence of $F_2^{D(4)}(\xi, \beta, Q^2, t)$ on Q^2 is found to be weak in the data, in good agreement with our results. Remember that our calculation is at Born level and does not incorporate the effects of QCD evolution of structure functions.

Regarding the overall normalisation we find that agreement is not too bad given that we have done a leading order calculation and taking into account the uncertainty in its normalisation due to the strong coupling at different scales we discussed in Sect. 2. We also stress that the parameters of our model, β_0^2, μ_0^2 and $\alpha_s^{(0)}$, have all be determined from pre-HERA data and that in this sense our prediction is parameter free. As to the shape in β the data clearly do not show a decrease at small β as our result does. This is not surprising since we only calculate the $q\bar{q}$-component of the diffractive final state, and at small values of β, i.e. at large diffractive mass M final states with additional gluons are expected to be dominant. Figure 6 indicates that this might be the case for values of β well above 0.1. We remark that the more recent ZEUS data [18] indicate a rise of $F_2^{(D)4}$ as β becomes small whereas the preliminary H1 data [19] give a very flat behaviour over the entire β-range.

In Fig. 7 we compare the predictions of the model for $F_2^{I\!P}(c\bar{c})$ and $F_2^{I\!P}$ for the three light flavours, keeping in mind that neither is expected to be a complete description at small β. The curves for light quarks are scaled down by a factor of 20. The fraction of charm comes out quite small,[2] it is not larger than 5% and decreases with β. For

[2] The results for the charm contribution to the diffractive structure function presented here are significantly smaller than

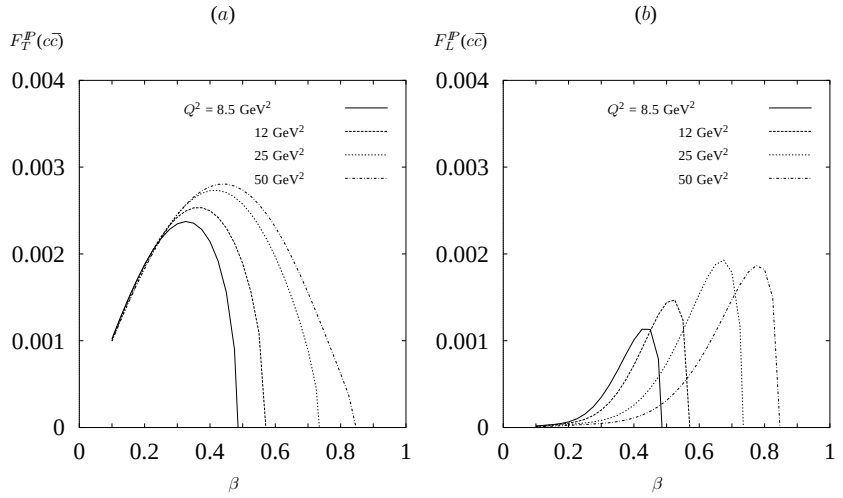

Fig. 5. Charm structure functions $F_T^{I\!P}(c\bar{c})$, $F_L^{I\!P}(c\bar{c})$ of the pomeron for transverse and longitudinal photon polarisation at different values of Q^2

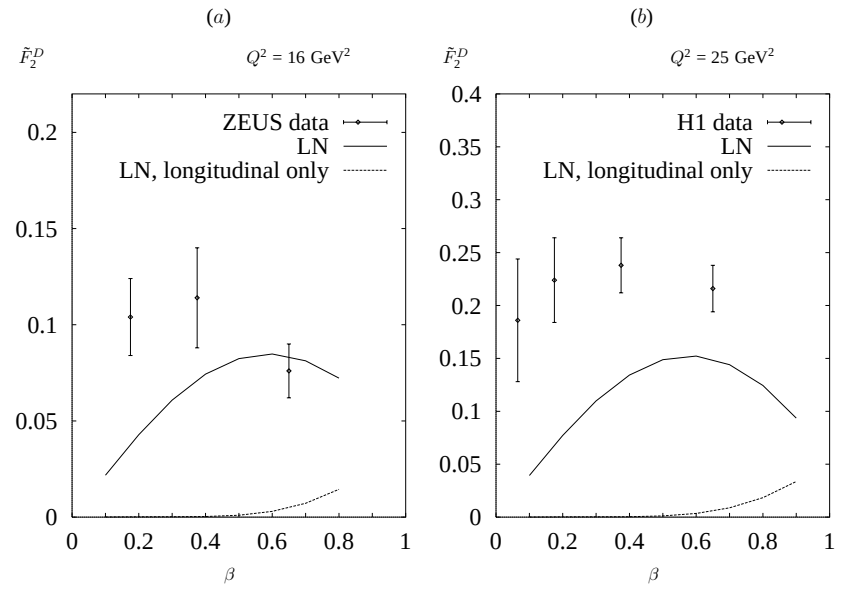

Fig. 6. HERA data [17] for the ξ-integrated diffractive structure function $\tilde{F}_2^D(\beta, Q^2) = \int_{\xi_{min}}^{\xi_{max}} d\xi \int dt\, F_2^{D(4)}(\xi, \beta, Q^2, t)$ compared with the result in the LN model. Also shown is the longitudinal contribution $\tilde{F}_L^D$ to $\tilde{F}_2^D$. Integration limits are $\xi_{min} = 6.3 \cdot 10^{-4}$, $\xi_{max} = 0.01$ in the case of ZEUS and $\xi_{min} = 3 \cdot 10^{-4}$, $\xi_{max} = 0.05$ for the H1 data

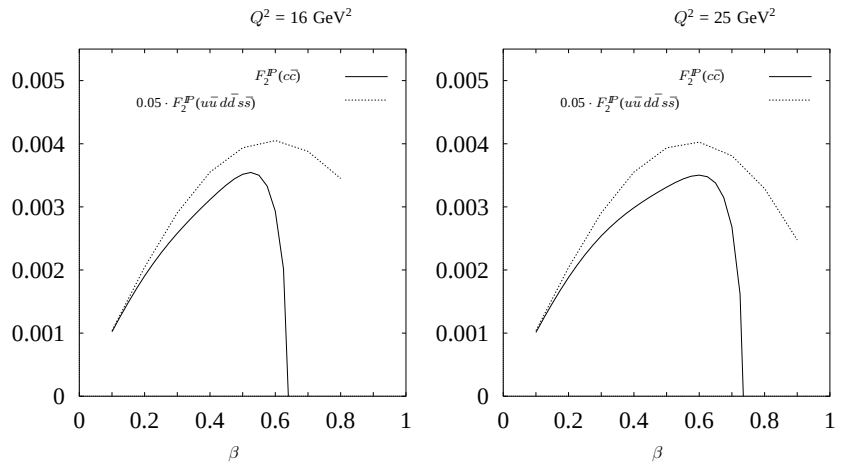

Fig. 7. Pomeron structure function $F_2^{I\!P}(c\bar{c})$ for charm compared with 0.05 times $F_2^{I\!P}$ for the three light flavours. **a** for $Q^2 = 16$ GeV^2 and **b** for $Q^2 = 25$ GeV^2

$\beta \gtrsim 0.4$, where we expect the $q\bar{q}$-component to dominate the final state, we find the fraction of charm in $F_2^{I\!P}$ to be below 4%.

We observe that for the *longitudinal* pomeron structure function the contribution of charm can be considerable. It is largest for β around 0.5 where the ratio between $F_L^{I\!P}(c\bar{c})$ and $F_L^{I\!P}$ for all flavours can reach values close to 0.6. This is larger than the ratio of the squared electric charges so that apart from the charge the cross section for charm exceeds that of a light $q\bar{q}$-pair. Note that the differential longitudinal cross section has a suppression factor $(P_T^2 + m_q^2)/M^2$ at small P_T^2 which is less efficient for large quark mass m_q. This phenomenon should however be difficult to observe since the longitudinal part of $F_2^{I\!P}$ is tiny at $\beta \sim 0.5$ and only visible at rather high β and not too large Q^2, where M^2 is below the charm threshold.

To conclude we wish to report an observation regarding the ratio of the rates for diffractive $c\bar{c}$- and $b\bar{b}$-production. We compare the integrated cross sections for photoproduction, so that the scale Q^2 cannot influence this ratio, taking $W = 220$ GeV and imposing $\xi \leq 0.05$. We checked that at this W the effect of the phase space reduction through the cut in ξ is about the same for charm and bottom: calculating the cross sections for very high W where the ξ-cut has no effect we verified that the increase of the cross sections is almost entirely due to the factor $W^{4(\alpha_{I\!P}-1)}$ from pomeron exchange. With $m_c = 1.5$ GeV and $m_b = 4.5$ GeV we find that the cross section for bottom production is about 440 times smaller than for charm, implying that this process should be quite impossible to observe at HERA. Taking out the squared electric charges and the running strong coupling, which for simplicity we take here at fixed scales m_c^2 or m_b^2, we obtain

$$\frac{\sigma(\gamma p \to c\bar{c}\, p)}{\sigma(\gamma p \to b\bar{b}\, p)} \cdot \frac{e_b^2\, \alpha_s(m_b^2)}{e_c^2\, \alpha_s(m_c^2)} \approx 71 \approx \left(\frac{m_b}{m_c}\right)^{3.9} . \qquad (18)$$

Apart from the effect of the running coupling the integrated cross section appears to scale with the quark mass approximately like $1/m_q^4$. To check this we have calculated the photoproduction cross section as a function of m_q between $m_q = 1.5$ GeV and 15 GeV, for very large W so that the ξ-cut has no effect. Dividing by the running coupling $\alpha_s(m_q^2)$ we find indeed an approximate power behaviour in $1/m_q$ with an exponent between 3.6 and 4.2. A behaviour in $1/m_q^4$ looks like the effect of the off-shell propagators in the amplitude whose denominators are limited by m_q^2. Notice that the numerators of the propagators, which also contain one power of m_q do not seem to enter in the same way, their role is more complicated because the numerator of a quark propagator has a Dirac matrix structure.

4 Summary

We have calculated diffractive production of a $c\bar{c}$-pair in $\gamma^* p$ collisions with real or virtual photons in the model of nonperturbative two-gluon exchange due to Landshoff and Nachtmann. This allowed us to give numerical predictions for diffractive charm production at HERA, for cross sections and spectra in M^2 and P_T^2.

In photoproduction we find a γp cross section in the region of 60 nb for W around 200 GeV. The mass spectrum peaks at rather low values of M and then falls off roughly like $1/M^4$, whereas the spectrum of the transverse momentum approximately behaves like a power of $P_T^2 + m_c^2$ with an exponent around -4.

In diffractive DIS the ep cross section we obtain is of order 100 pb for Q^2 from 7.5 GeV^2 to 80 GeV^2 and W from 50 GeV to 220 GeV. The $\gamma^* p$ cross sections exhibit a flat dependence on W, typical of models with soft pomeron exchange. We suggest that even a coarse logarithmic binning in W of the ep cross section should be useful to test this in the data.

Expressing the $c\bar{c}$ mass spectra in terms of the diffractive charm structure functions we find that the transverse contribution $F_T^{D(4)}(c\bar{c})$ does not scale for $\beta \gtrsim 0.3$ due to the restricted phase space at HERA values of Q^2. The longitudinal structure function $F_L^{D(4)}(c\bar{c})$ for charm is comparable to the transverse one at small diffractive mass M, i.e. close to the largest kinematically allowed β at given Q^2, at lower β it is negligible.

We have then compared $F_2^{D(4)}(c\bar{c})$ with the diffractive structure function $F_2^{D(4)}$ for light flavours, calculated in the same model, which reproduces the HERA data within a factor of 2 or so, except in the region of small β where the neglect of final states other that $q\bar{q}$ becomes a bad approximation. The contribution of $c\bar{c}$ to the diffractive structure function $F_2^{D(4)}$ comes out below 5% in our model.

The strong quark mass dependence of the integrated $q\bar{q}$ cross section can be understood in a simple way from the denominator of the propagator for the off-shell quark in the Feynman diagrams, which appears squared in the cross section. Its typical value is given by $\langle \lambda^2 \rangle = (\langle P_T^2 \rangle + m_q^2)/(1-\beta)$, where $\langle P_T^2 \rangle$ is some average P_T^2. For photoproduction of heavy quarks we find indeed a quark mass dependence of the cross section approximately like $1/m_q^4$, which together with the effect of the running strong coupling and the different quark charges leads to a ratio of $b\bar{b}$- to $c\bar{c}$-production of 1/440.

Acknowledgements. I am grateful to P V Landshoff for his continued interest in this work and for many conversations. Thanks are also due to I T Drummond and H Lotter for discussions. This work was initiated by the DESY workshop on "Future Physics at HERA" and I would like to thank the conveners of the working group on "Hard diffractive processes", H Abramowicz, L Frankfurt and H Jung, for the stimulating and pleasant atmosphere during the workshop.

I acknowledge the financial support of the EU Programme "Human Capital and Mobility", Network "Physics at High Energy Colliders", Contracts CHRX-CT93-0357 (DG 12 COMA) and ERBCHBI-CT94-1342.

those given in [11] because there we used the running coupling $\alpha_s(P_T^2)$ which unlike $\alpha_s(\lambda^2)$ is not limited from above by $\alpha_s(m_c^2)$ and was frozen when it reached the value 1

References

1. ZEUS Collaboration, Phys. Lett. B315 (1993) 481;
   H1 Collaboration, Nucl. Phys. B429 (1994) 477
2. G Briskin and M F McDermott, "Diffractive Structure Functions in DIS" in: *Future Physics at HERA*, Proc. of the workshop 1995/96, eds. G Ingelman, A De Roeck and R Klanner, DESY 1996
3. T Gehrmann and W J Stirling, Z. Phys. C70 (1996) 89
4. M Genovese, N N Nikolaev and B G Zakharov, Phys. Lett. B378 (1996) 347
5. E M Levin, A D Martin, M G Ryskin and T Teubner, Durham preprint DTP-96-50, hep-ph/9606443
6. H Lotter, DESY–96–260, hep-ph/9612415
7. P V Landshoff and O Nachtmann, Z. Phys. C35 (1987) 405
8. A Donnachie and P V Landshoff, Nucl. Phys. B311 (1988/89) 509
9. J R Cudell, A Donnachie and P V Landshoff, Nucl. Phys. B322 (1989) 55
10. J Bartels, H Lotter and M Wüsthoff, Phys. Lett. B379 (1996) 239
11. M Diehl, Z. Phys. C66 (1995) 181
12. M Diehl, Palaiseau preprint CPTH-S472-1096, hep-ph/9610430
13. A Donnachie and P V Landshoff, Nucl. Phys. B267 (1986) 690
14. J R Cudell, Nucl. Phys. B336 (1990) 1
15. G Ingelman and P Schlein, Phys. Lett. B152 (1985) 256
16. M Diehl, "Diffraction in electron-positron collisions", Ph. D. thesis, University of Cambridge, 1996 (unpublished)
17. H1 Collaboration, Phys. Lett. B348 (1995) 681;
    ZEUS Collaboration, Z. Phys. C68 (1995) 569
18. ZEUS Collaboration, Z. Phys. C70 (1996) 391
19. H1 Collaboration, S Tapprogge et al., "Diffractive deep inelastic scattering", Talk given at the 31st Rencontres de Moriond: QCD and high-energy hadronic interactions, Les Arcs, France, 23–30 March 1996, hep-ex/9605007